Preparation, stability, and in vitro transport of soybean protein-based diosgenin nanoemulsions

Li Guanghui [a,1], Liu Qi [b,1], Gao Anning [c], Ren Luting [b], Zhang Yinghan [b], Guo Weiyun [a], He Shenghua [a], Gao Fengyi [c,*], Peng Xiaoli [b,*]

[a] Food and Pharmacy College, Xuchang University, Xuchang, Henan 461000, China
[b] College of Food Science and Engineering, Northwest A&F University, Yangling, Shaanxi 712100, China
[c] College of Biology and Food, Shangqiu Normal University, Shangqiu, Henan 476000, China

ARTICLE INFO

ABSTRACT

Soybean protein isolate (SPI)-stabilized nanoemulsions (NEs) were formulated to encapsulate diosgenin (DIO) to enhance its water solubility and bioavailability. The influence of DIO concentrations on NEs' properties was investigated, and their environmental stability and cell permeability were also assessed. Results demonstrated that DIO significantly affected all the physicochemical properties of NEs. NEs with 1.0 mg/mL of DIO exhibited smaller droplet size (209 nm), lower polydispersity index (0.17), and higher stability coefficient (95.8 %). Furthermore, DIO-SPI NEs displayed better stability under appropriate pH (<4 or > 5), NaCl concentrations (≤ 0.3 M), temperatures (≤ 60 °C), and freeze–thaw cycles (≤ 2), as well as storage at 4 °C. Moreover, encapsulating DIO in NEs reduced its toxicity towards cells and enhanced its transport efficiency, which reached $3.16 \sim 4.87 \times 10^{-6}$. These findings highlight the potential of SPI-based NEs as a promising carrier for the efficient delivery of DIO.

1. Introduction

Diosgenin (DIO), a natural steroid sapogenin, is widely found in plants such as *Smilax china, Dioscorea rhizome,* and *Trigonella foenum graecum* (C. Liu et al., 2017). It processes various health-promoting and disease-preventive/therapeutic effects, including antioxidant, anti-inflammatory, anti-cancer, hypolipidemic, hypoglycemic, neuro-protective, *etc.* (Semwal et al., 2022; Wu & Jiang, 2019). However, DIO's poor water solubility and low bioavailability limit its application in food and pharmaceutical products. Many efforts have been made to enhance the solubility and bioavailability of DIO. Okawara et al. (2014) discovered that the combination of liquid crystals and β-cyclodextrin effectively improved the bioavailability of DIO. Li et al. (2015) demonstrated that amphiphilic conjugates poly (ethylene glycol)-DIO can substantially improve both the solubility and bioavailability of DIO. Liu et al. (2017) observed that DIO nanocrystals with a size of 229 nm exhibited a rapid and increased dissolution rate, leading to enhanced oral bioavailability compared with raw DIO.

Nanoemulsions (NEs) are described as optically transparent or translucent colloidal delivery systems with two immiscible phases (Heydari Gharehcheshmeh, Arianfar, Mahdian, & Naji-Tabasi, 2021). One phase is dispersed as discontinuous droplets with diameters ranging from 20 to 500 nm (the dispersed phase), while the other exits as the continuous phase (Walia & Chen, 2020). Due to their nanometric size and larger surface area, NEs have several remarkable advantages in carrying and delivering biologically active compounds compared to conventional emulsions (the diameter of the dispersed phase < 200 μm). Some of these advantages include improving water solubility, environment stability, and enhancing bioavailability, enabling controlled release in the gastrointestinal tract (Artiga-Artigas, Acevedo-Fani, & Martín-Belloso, 2017; Walia et al., 2020). Recently, numerous NEs loaded with bioactive substances such as resveratrol (Chunhong Li, Wang, Lei, & Zhang, 2023), curcumin (Gonçalves, Vicente, & Pinheiro, 2023; Shahbazizadeh, Naji-Tabasi, & Shahidi-Noghabi, 2022), luteolin (Karami-Mohajeri, Hashemi, Ranjbar, Mohajeri, & Sharififar, 2023), and β-carotene (Geng et al., 2023) have been extensively reported. However, the thermodynamic instability of NEs can result in creaming, sedimentation, aggregation, flocculation, and the Ostwald phenomenon

---

(Marhamati, Ranjbar, & Rezaie, 2021). Emulsifiers, hydrophilic and lipophilic surfactants, are extensively used to enhance the stability of emulsions. At present, synthetic surfactants such as tweens and spans are commonly employed in the formulating of NEs. However, due to their toxicity concerns, natural surfactants, including carbohydrates (chitin, starch, etc.), proteins (pea protein, zein, soy protein, etc.), and hydro-colloids (gum, pectin, etc.), have gained increasing attention (Marha-mati et al., 2021). Among these natural emulsifiers, plant proteins like rice bran protein, soybean protein isolate (SPI), and pea protein have become particularly attractive due to their safety and sustainability as well as the dietary preferences of vegetarians (Chen et al., 2020; Walia *et al.*, 2020; Yangying Zhou et al., 2022).

SPI, which possesses both hydrophobic and hydrophilic groups, plays an essential role in the preparation of NEs as an emulsifier (Hu, Xie, Zhang, Li, & Qi, 2020; Xu, Mukherjee, & Chang, 2018). Due to its biocompatibility, biosecurity, film-forming capabilities, and cost-effectiveness, SPI has been widely used for stabilizing emulsion systems. Several studies have been reported on the formulation and prop-erties of SPI-based NEs. Zhou et al. (2022) discovered that high-pressure homogenization and sodium alginate enhanced SPI-based NEs' thermal stability and storage stability. Wang et al. (2022) used a flash nano-precipitation method to fabricate lutein-loaded SPI nanoparticles, which exhibited a small particle size (80 ~ 122 nm), a narrow size distribution (PDI ~ 0.2), excellent stability, and improved bioaccessibility of lutein. Jin et al. (2021) demonstrated that emulsions formulated with 0.5 mg/mL nervonic acid and 1.5 wt% SPI under pressure conditions (120 MPa, 5 cycles) contained nano-scale droplets and displayed significant rheo-logic properties. Hu et al. (2020) observed that the perilla oil NEs sta-bilized by 3 % SPI exhibited superior physicochemical properties and stability.

The objective of this study was to use SPI to stabilize medium-chain triacylglycerol oil (MCT)-in-water (O/W) NEs as the nanocarrier for DIO and evaluate the Z-average diameters, zeta-potential, polydispersity index (PDI), stability coefficient (R), encapsulation efficiency (EE), rheology behavior, and microstructure of the DIO-loaded SPI-stabilized NEs (DIO-SPI NEs). Moreover, the impact of pH, NaCl concentration, thermal treatment, freeze–thaw cycles, and storage on the properties of DIO-SPI NEs was also explored. Finally, the cytotoxicity and cell permeability of DIO-SPI NEs were determined using Caco-2 cells.

2. Materials and methods

2.1. Materials and reagents

SPI ($\geq$92 %) and MCT ($\geq$99 %) were obtained from Shanghai Yuanye Biotechnology Co., Ltd. (Shanghai, China). DIO ($\geq$98 %) was purchased from Nanjing Chunqiu Biological Engineering Co., Ltd. (Nanjing, China). Nile red and Nile blue ($\geq$85 %) were bought from Sigma-Aldrich (Saint Louis, USA). Dulbecco's Modified Eagle's Medium (DMEM) and Hank's balanced salt solution (HBSS) were purchased from Shanghai BasalMe-dia Technologies Co., Ltd. (Shanghai, China). Fetal bovine serum (FBS) was obtained from Hyclone (Logan, USA). Penicillin-streptomycin so-lution, trypsin, and dimethyl sulfoxide (DMSO) were purchased from Beyotime Biotech. Inc. (Shanghai, China). Methyl Thiazolyl Tetrazolium (MTT) was from Beijing Solarbio Science & Technology Co., Ltd. (Bei-jing, China). All other chemicals were of analytical reagent grade and were obtained from Beijing Chemical Works (Beijing, China).

2.2. Preparation of DIO-SPI NEs

DIO-SPI NEs were prepared using the method reported by Bu et al. (2023) with minor modifications. In brief, the SPI (4 %, w/v) was dis-solved in ultrapure water and stirred at room temperature until completely dissolution. The oil phase was developed by dispersing different concentrations of DIO in MCT oil, followed by stirring at room temperature for 40 min. The aqueous phase was mixed with the oil

phase at a ratio of 9:1 (v/v) and then stirred for 2 h at room temperature to achieve complete dispersion. Subsequently, the mixture was ho-mogenized for 3 min at 12,000 rpm using a homogeneous dispersing machine (Ultra-Turrax T25, IKA, Staufen, Germany) to form coarse emulsions, followed by homogenization using a high-pressure homog-enizer (GJJ-0.05/60, Shanghai NONI Light Industry Machinery Co., Ltd., Shanghai, China) at 50 MPa for three cycles to obtain the NEs. The final concentrations of DIO in the NEs were 0.8, 0.9, 1.0, 1.1, and 1.2 mg/mL, respectively.

2.3. Characterization of DIO-SPI NEs

2.3.1. Z-average diameters, zeta-potential and polydispersity index

The Zetasizer Nano-ZS (ZEN 3600, Malvern, UK) was used to analyze the Z-average diameters, zeta-potential, and PDI of the DIO-SPI NEs. The samples were diluted 300-fold with ultrapure water to eliminate mul-tiple scattering effects. The instrument parameters were: He-He as a laser, wavelength 633 nm, scattering angle 173°, refraction rate 1.40, and ultrapure water as the dispersant (Chen et al., 2020).

2.3.2. Stability coefficient

With some modifications, the method reported by Chen et al. (2020) was used to determine the R of DIO-SPI NEs. Briefly, 2 mL of samples were centrifuged (3000 g, 15 min) in a centrifuge tube. The subnatant was collected and diluted 100-fold using ultrapure water. The absor-bance was determined at 410 nm, and the R was calculated as follows:

$$R(\%) = \frac{A_1}{A_0} \times 100\%$$

where A_0 was the NEs absorbance before centrifugation, and A_1 was the subnatant absorbance after centrifugation.

2.3.3. Encapsulation efficiency

The EE of DIO-SPI NEs was determined according to the method published by Zhou et al. (2020) with slight modifications. Samples (0.5 mL) were added to 12.0 mL of DMSO and centrifuged at 3000 *g* for 15 min. The absorbance of the supernatant was measured at 410 nm. The EE was calculated as follows:

$$EE(\%) = \frac{M_0 - M_1}{M_0} \times 100\%$$

where M_0 was the total weight of the DIO initially added, and M_1 was the weight of the free DIO.

2.3.4. Rheological properties

The rheological behavior of the DIO-SPI NEs was determined at 25 °C using a Discovery hybrid rheometer (DHR-1, TA, USA), following the method described by Zhou et al. (2022). The parameters were: 40 mm plate geometry, 1.0 mm gap, and 0.1 ~ 500 1/s shear rate.

2.3.5. Microstructural observation

Using confocal laser scanning microscopy (CLSM) (TCS SP8, Leica, Germany), the microstructure of DIO-SPI NEs was evaluated. The fluo-rescent dye mixture (40 μL; 0.01 % Nile red and 0.1 % Nile blue) and NEs (360 μL) were incubated in the dark for 20 min. Then, 10 μL of the sample was placed on a glass slide and covered with a slip. Images were immediately taken using a 63 × magnification lens and excitation wavelengths of 488 and 633 nm (Bu et al., 2023).

2.3.6. Turbidity

According to the method of Zhou et al. (2022), the DIO-SPI NEs were diluted 100 times with ultrapure water. The turbidity was determined at 600 nm using a UV-2600 spectrophotometer. Ultrapure water was used as a blank.

2.4. Stability of DIO-SPI NEs

2.5.1. pH stability

The DIO-SPI NEs were prepared at different pH levels (2 ~ 10) by adjusting the samples with hydrochloric acid (1 M) or sodium hydroxide (1 M). Samples were kept at room temperature for 2 h and then diluted 100 times before analysis (Falleh, Jemaa, Neves, Isoda, Nakajima, & Ksouri, 2021a).

2.5.2. NaCl stability

The DIO-SPI NEs (5 mL) were mixed with the NaCl solution, and the final NaCl concentration ranged from 0 to 0.5 mol/L. Samples were then stored at room temperature for 2 h before use (Falleh et al., 2021a).

2.5.3. Thermal stability

The DIO-SPI NEs were placed in a centrifuge tube and then heated in a water bath at 60, 80, and 100 °C for 30 min, respectively. Subsequently, the samples were cooled down for 90 min before analysis.

2.5.4. Freeze-thaw stability

The DIO-SPI NEs were poured into a glass bottle and stored at − 18 °C for 20 h. Then, the samples were subjected to 3 thawing cycles at room temperature for 2 h. The properties of the NEs were immediately determined after each cycle (Tian et al., 2021).

2.5.5. Storage stability

The DIO-SPI NEs were stored at 4, 25, and 37 °C for 30 days. The NEs were sampled every 5 days to evaluate their properties.

2.6. Caco-2 cell culture model

Caco-2 cells were cultured and maintained in a humidified incubator (37 °C, 5 % CO$_2$, and 90 % relative humidity) using DMEM containing sodium pyruvate and high glucose supplemented with 10 % FBS and 1 % double-antibody.

2.6.1. Cytotoxicity assay

The MTT assay was used to explore the safety of the DIO-SPI NEs (Walia *et al.*, 2020). The DIO were dissolved in DMEM containing 1 ‰ DMSO. Caco-2 cells in the logarithmic growth phase were seeded in 96-well plates at a density of 10^5 cells per well and incubated for 12 h. After removing the supernatant, the DIO-SPI NEs and DIO solutions were added to each well. Following a 24-h incubation, the solution was removed and washed away with PBS. In each well, 10 μL of MTT solvent (0.5 mg/mL in DMEM) was added and incubated for 4 h at 37 °C, followed by discarding the MTT solution. Subsequently, 150 μL of DMSO was added and shaken for 20 min. A microplate reader (M200 pro, TECAN, Sweden) was used to determine the absorbance at 570 nm, and cell viability was expressed as a percentage of living cells in the test wells compared to the control wells.

2.6.2. Caco-2 cell monolayers

According to the method described by Yang, Wang, & Li (2019), Caco-2 cell monolayers were obtained by seeding cells onto polycarbonate membrane filters (0.4 μm pore size, 12 mm diameter) inside Transwell 12-well plates at a density of 1×10^5 cells per well. Subsequently, 0.5 mL of DMEM was added to the apical side (side A), and 1.5 mL of DMEM was added to the basolateral side (side B), followed by incubation in a humidified incubator (37 °C, 5 % CO$_2$, and 90 % relative humidity). The medium was changed after 24 h, and afterwards every second day for the next 21 days. To establish integral monolayers, transepithelial electrical resistance (TEER) values were assessed using an epithelial voltammeter. Monolayers with TEER values over 200 Ω/cm^2 were considered suitable for transport studies.

2.6.3. Transport efficiency

After 21 days, the DMEM in sides A and B was removed, and the cell monolayers were washed twice with HBSS. The Transwell plate was then placed in an incubator for 1 h. Subsequently, the HBSS in both sides was completely drained. Next, 0.5 mL of HBSS containing either DIO or DIO-SPI NEs was added to side A, while 1.5 mL of HBSS was added to side B. HBSS alone was used as the control. After incubating at 37 °C for 0, 1, 2, 3, and 4 h, samples (0.6 mL) from each basolateral chamber were collected and then replaced with fresh HBSS solution (0.6 mL). The samples were stored at −80 °C until use. The apparent permeability coefficient of the DIO was calculated as follows:

$$P_{app} = \frac{dQ}{dt(A \times C_0)}$$

where dQ was the total amount of the DIO permeating through the cell monolayer, dt was the test time, A was the membrane area per well of the Transwell plate (1.21 cm^2), and C$_0$ was the initial DIO concentration.

2.7. Statistical analysis

Experiments were carried out in triplicate, and the data were described as the mean ± standard deviation. Single-factor analysis of variance (ANOVA) was used for statistical comparisons, and a $p < 0.05$ was considered significant.

3. Results and discussion

3.1. Characterization of DIO-SPI NEs

Natural products at varying dosages exert significant effects on the droplet size and EE of emulsions (Chen et al., 2020; El Fagui & Amiel, 2012). To obtain NEs with smaller droplet sizes and higher EE, the effect of DIO concentration on the properties of NEs was researched. As shown in Fig. 1**A**, the Z-average diameters of the DIO-SPI NEs ranged from 209 nm to 300 nm. Notably, increasing the DIO concentration from 0.8 mg/mL to 1.0 mg/mL led to a significant reduction in the Z-average diameters. This may be due to the DIO, a lipophilic active substance, which could tightly aggregate oil together, resulting in smaller droplets. However, a further increase in the amount of DIO from 1.0 mg/mL to 1.2 mg/mL resulted in larger droplet sizes. This increase can be explained by the fact that the excess of the DIO may precipitate out and destroy the structure of the NEs. The results were in disagreement with Chen et al. (2020), Falleh et al., (2021b), and Pandey et al. (2015), who showed an increase in the droplet size of NEs with increasing the concentration of natural products.

Zeta-potential is a critical parameter describing the repulsion or attraction between the droplets in the emulsion. The larger the absolute value of the Zeta-potential, the higher the stability of the NEs (Tian et al., 2021). All the DIO-SPI NEs showed negative Zeta-potential values, indicating the presence of negatively charged groups on the outer layer of droplets resulting from the SPI (Fig. 1**B**). The NEs with 0.9 mg/mL DIO displayed the highest absolute zeta-potential (29.5 mV), followed by NEs carrying 1.0 mg/mL DIO (25.0 mV), suggesting more excellent stability than other treatments.

The PDI reflects the distribution homogeneity of the droplet size, and PDI values ≤ 0.3 indicate a homogenous system. The PDI values for treatments at 0.8, 0.9, 1.0, 1.1, and 1.2 mg/mL were 0.36, 0.18, 0.17, 0.35, and 0.32, respectively, indicating all NEs were uniformly distributed (Fig. 1**C**). NEs containing 1.0 mg/mL DIO showed the minimum PDI (0.17). These results agreed with López-Monterrubio et al. (2021), who reported that the PDI values of β-carotene NEs stabilized by whey protein hydrolyzate and high methoxyl pectin soluble complex were < 0.25. In addition, the R of the DIO-SPI NEs was maintained between 92.3 % and 95.8 % as the DIO concentration increased, indicating excellent stability of the NEs (Fig. 1**D**).
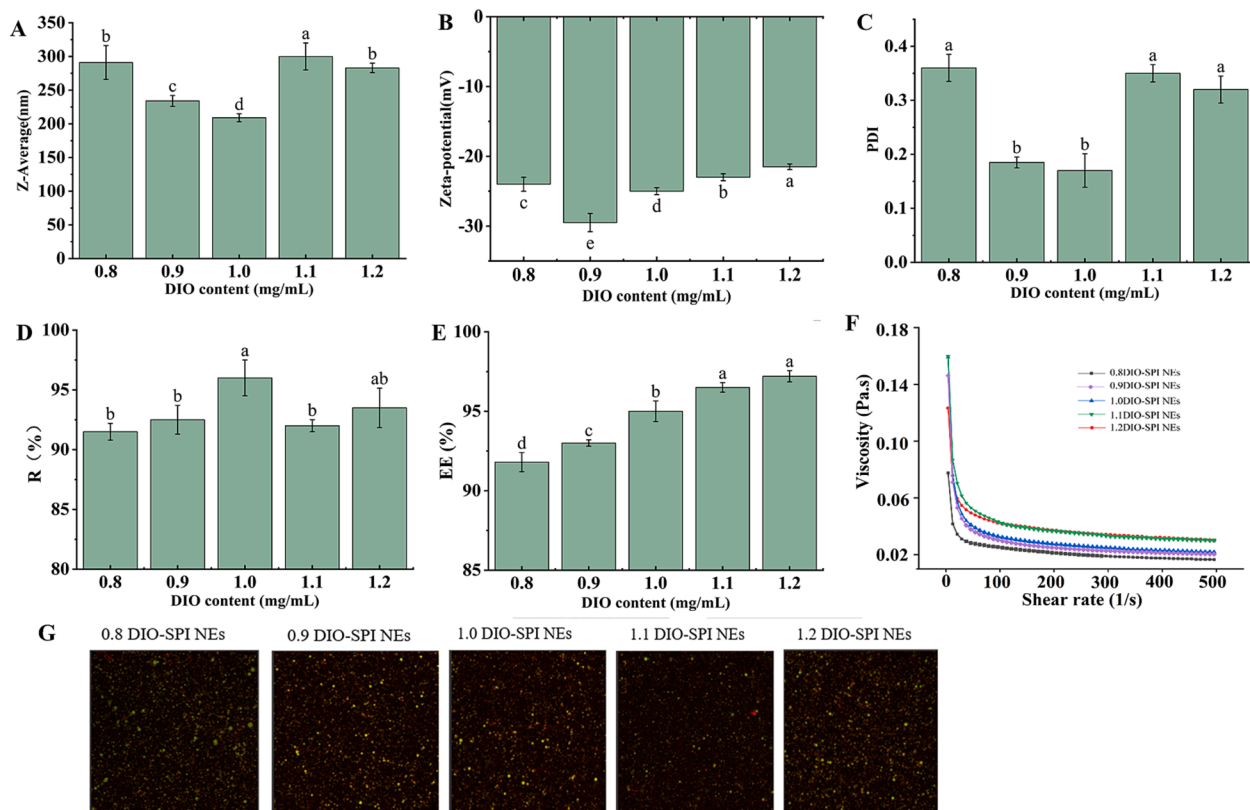
Fig. 1. Effect of DIO concentration on the characteristics of DIO-SPI NEs. (A) Z-Average; (B) zeta-potential; (C) PDI; (D) R; (E) EE; (F) viscosity; (G) microstructure. Bars (mean ± std dev, n = 3) with different letters have mean values that are significantly different (p < 0.05). DIO, diosgenin; NEs, nanoemulsions; SPI, soybean protein isolate; PDI, polydispersity index; R, stability coefficient; EE, encapsulation efficiency.

As seen in Fig. 1**E**, as the DIO concentration increased, the EE of the DIO-SPI NEs increased from 91.8 % to 97.2 %. This result was in accordance with previous studies showing an improvement in the EE of NEs as the loading substance increased (Chen et al., 2020; Pandey et al., 2015). Due to the > 91 % embedding rate in each treatment, DIO-SPI NEs can be regarded as an efficient encapsulation system. Based on these findings, 1 mg/mL of DIO was ideal for producing DIO-SPI NEs with a Z-average diameter of 209 nm and an EE of 94.9 %.

3.2. Rheological properties

The viscosities of NEs containing 0.8 ~ 1.2 mg/mL DIO are shown in Fig. 1**F**. All the DIO-SPI NEs exhibited shear thinning behaviour within a shear rate range of 0 to 100 1/s, indicating severe structural damage in the NEs. This was associated with the deflocculation of oil droplets. However, because of the insensitivity of viscosity, the viscosity of DIO-SPI NEs was relatively stable at shear rates of 100 ~ 500 1/s. These findings agreed with previous studies on the tuna fish oil NEs carrying curcumin and resveratrol (Shehzad et al., 2021) and capsaicin NEs (Yan Zhou et al., 2020). Significantly, NEs containing 1.1 mg/mL or 1.2 mg/mL DIO exhibited a more apparent viscosity than others with DIO ≤ 1.0 mg/mL, which might be related to the amount of DIO in NEs. For the NEs containing higher DIO, the DIO may precipitate from the oil phase as the increase in shear rate, thereby destroying the NEs' structure as well as the stable system formed by HHP. Subsequently, the NEs spontaneously emulsified to form larger droplets, leading to an increase in viscosity.

3.3. Microstructure

Fig. 1**G** displays the microstructure of the DIO-SPI NEs as determined by CLSM. The oil droplets were stained red, while the protein aggregates were depicted in blue. The proteins were flocculent, whereas the oil droplets appeared spherical and evenly distributed in the DIO-SPI NEs. Notably, NEs with 0.8, 1.1, and 1.2 mg/mL DIO displayed larger oil droplets and denser distribution. Conversely, NEs containing 0.9 and 1.0 mg/mL DIO showed smaller droplets and more uniform dispersion, which was consistent with Fig. 1**A**.
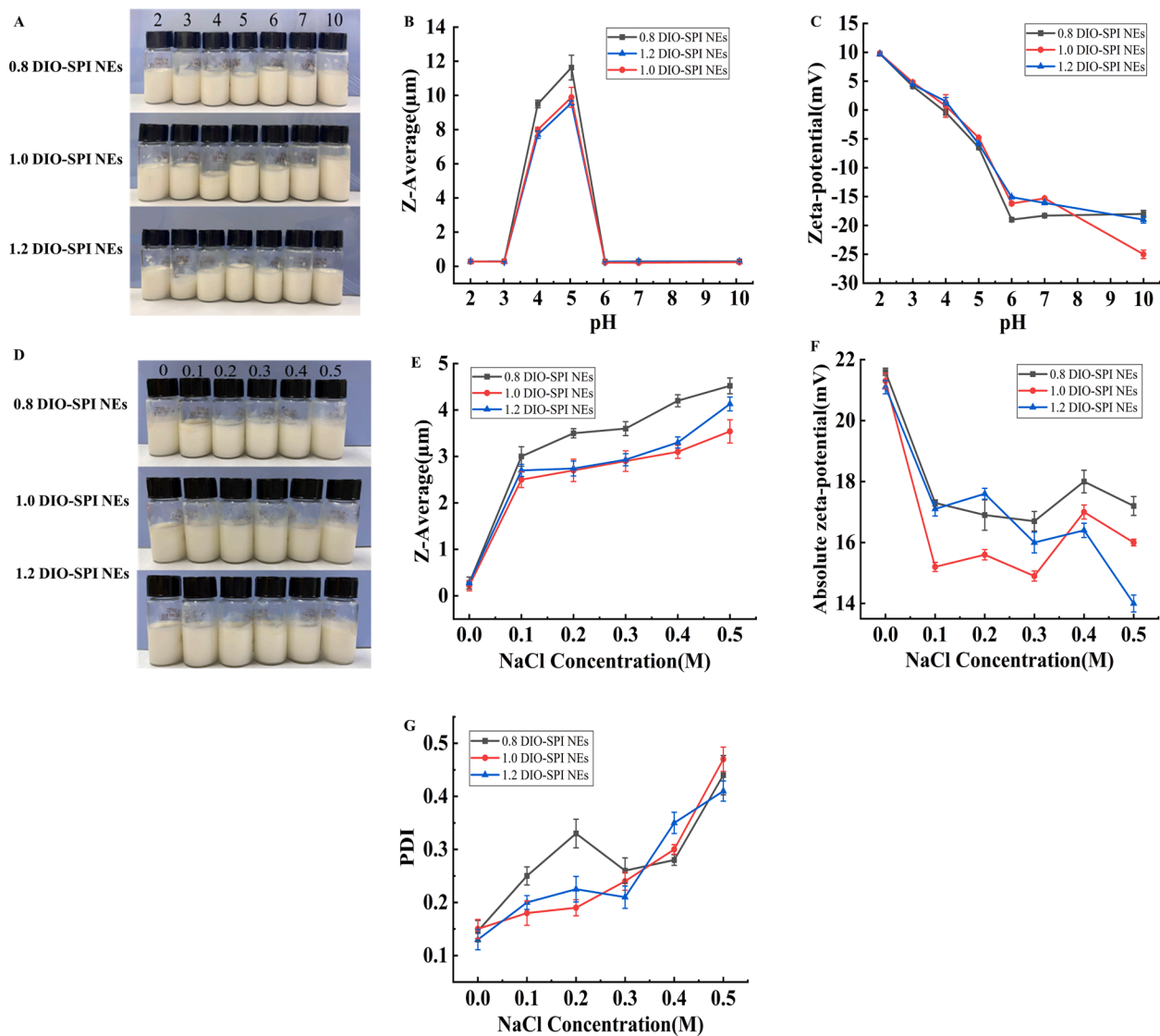
3.4. Stability of DIO-SPI NEs

3.4.1. pH stability

The effect of pH on the stability of DIO-SPI NEs is depicted in Fig. 2. The DIO-SPI NEs exhibited larger Z-average diameter at pH 4 and 5. However, DIO-SPI NEs displayed nanoscale Z-average diameters at pH <4.0 or pH > 5.0 (Fig. 2**B**). This was due to the SPI's isoelectric point (pI = 4.5). At the pI, SPI had poor solubility, and the electrostatic repulsion was weak in the system, leading to droplet aggregation (Fig. 2**A**). Similar results were found by Zhou et al. (2020) and Zhu et al. (2021). Zhou et al. (2020) found an increase in droplet size for both SPI-stabilized NEs and the SPI-Dex (40 kDa) mixture-stabilized NEs at the pI. Zhu et al. (2021) noted that resveratrol-loaded zein-polyglycerol conjugate-based NEs had the highest Z-average diameter and PDI values at pI = 4.0.

In addition, the zeta-potential of DIO-SPI NEs decreased from 10 mV to −25 mV as pH values increased from 2 to 10 (Fig. 2**C**), which can be attributed to the pI of SPI. Similar conclusions have been reported by Liao et al. (2021) and Tian et al. (2021), showing that the charge of the protein-stabilized NEs was positive below the pI and negative above the pI. The improved stability of the DIO-SPI NEs at various pH levels, except around the pI, was most likely due to the increased electrostatic repulsion among droplets.

3.4.2. NaCl stability

As shown in Fig. 2**D ~ G**, as the concentration of NaCl increased from 0 to 0.5 M, the Z-average diameter of the NEs loading 0.8, 1.0, and 1.2

Fig. 2. Effect of pH and NaCl on the stability of DIO-SPI NEs. pH stability: visual appearance (A), Z-Average(B), and zeta-potential (C); NaCl stability: visual appearance (D), Z-Average(E), zeta-potential (F), and PDI (G). DIO, diosgenin; NEs, nanoemulsions; SPI, soybean protein isolate; PDI, polydispersity index.

mg/mL DIO increased from 0.22 µm to 4.52, 3.54, and 4.13 µm, respectively; the absolute zeta-potential decreased from 21.6 mV to 17.2, 16.0, and 14.0 mV; and the PDI increased from 0.15 to 0.44, 0.47, and 0.41. The aggregation and flocculation of the DIO-SPI NEs caused by NaCl might be due to the van der Waals attraction forces between the protein-coated droplets (Sari et al., 2015). No significant differences were observed in Z-average diameter, PDI, and zeta-potential of the DIO-SPI NEs (p > 0.05) when NaCl concentration ranged from 0.1 to 0.2 M. However, as the concentration of NaCl increased from 0.3 to 0.5 M, the stability of the DIO-SPI NEs weakened, and droplet flocculation would be observed (as shown in Fig. 2D). Similar conclusions have been reported by Chen et al. (2020) and Liao et al. (2021). Chen et al. (2020) demonstrated that quercetin-rice bran protein NEs were stable at low NaCl concentrations (0 ~ 0.2 M) and unstable at 0.3 ~ 0.5 M. Liao et al. (2021) observed that the mean particle diameter of caseinate-stabilized NEs showed little change when exposed to NaCl concentrations ranging from 0 to 200 mmol/L, whereas NaCl at 300 mmol/L promoted an increase in particle size.
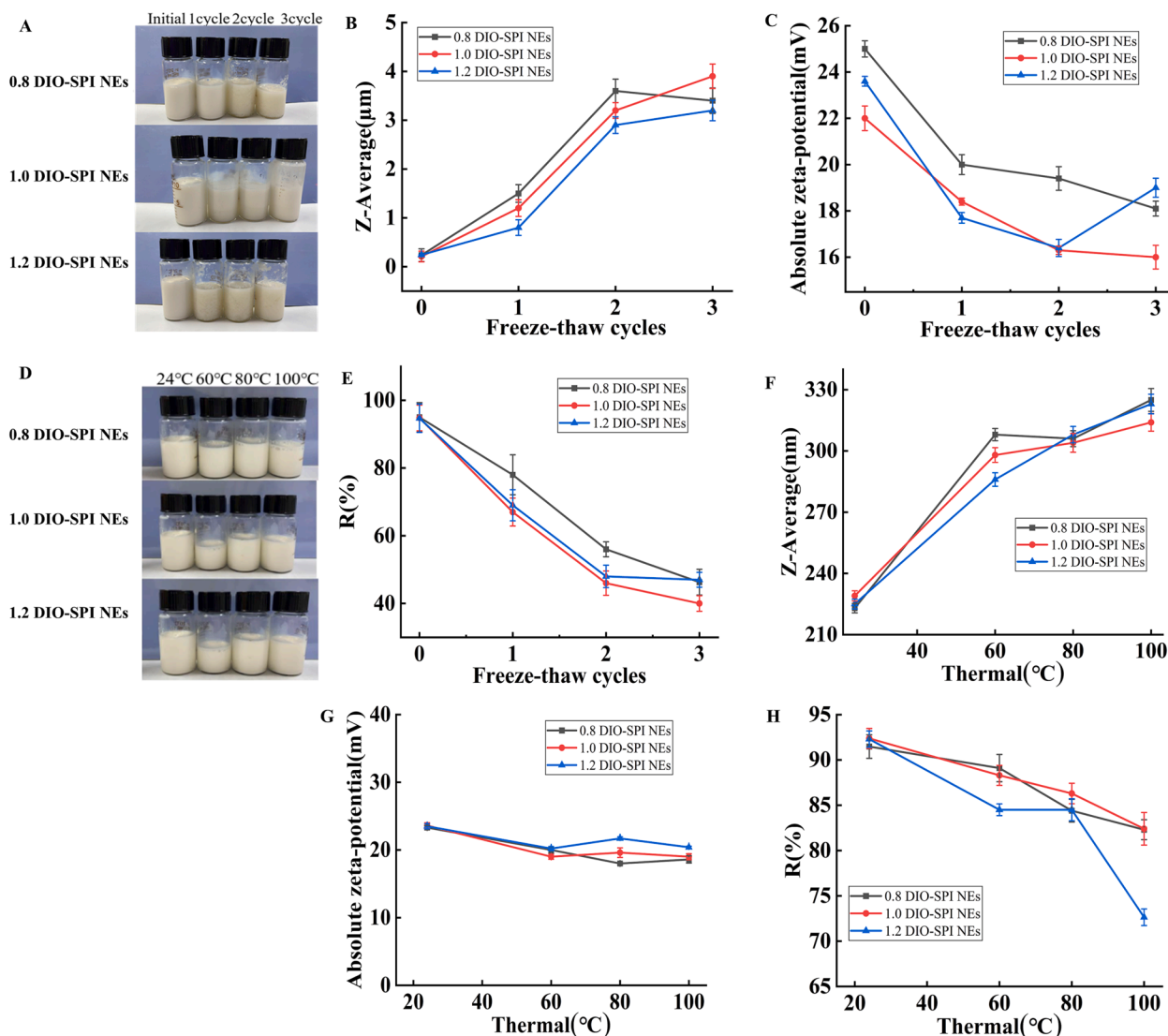
3.4.3. Freeze-thaw stability

As shown in Fig. 3, freeze–thaw treatment significantly affected the stability of DIO-SPI NEs. After freeze–thaw, the DIO-SPI NEs were more viscous, and flocculation appeared (Fig. 3A). As the number of freeze-–thaw cycles increased, the Z-average diameter of the DIO-SPI NEs increased from 0.209 ~ 0.300 µm to 3 ~ 4 µm (Fig. 3B). In cycle 2, there was a sharp increase in the Z-average diameter. This was primarily due to the fact that most of the water in the NEs froze, causing the oil droplets to separate out and aggregate. There was no significant increase in the Z-average diameter between cycles 2 and 3. The absolute zeta-potential decreased from 22 ~ 25 mV to 16 ~ 18 mV (Fig. 3C), and the R reduced from 95 % to 40 % (Fig. 3E). This was attributed to the freeze–thaw treatment, which resulted in the separation of SPI from NEs. It demonstrated that the NEs stabilized by a single protein had poor freeze–thaw stability. Our results agreed with Tian et al. (2021), who reported an increase in particle size and a decrease in absolute zeta-potential of SPI NEs after freeze–thaw treatment.

3.4.4. Thermal stability

The effect of thermal treatment (60, 80, and 100 °C) on the stability of DIO-SPI NEs was determined, and 24 °C was used as the control (Fig. 3). No apparent changes were found in the DIO-SPI NEs treated at 60, 80, and 100 °C for 30 min (Fig. 3D). The Z-average diameter of the DIO-SPI NEs increased as the temperature increased from 24 °C to 100 °C. This result may be due to the interfacial reaction between

Fig. 3. Effect of free-thaw and thermal on the stability of DIO-SPI NEs. Freeze-thaw stability: visual appearance (A), Z-Average(B), zeta-potential (C), and R (E); thermal stability: visual appearance (D), Z-Average(F), zeta-potential (G), and R (H). DIO, diosgenin; NEs, nanoemulsions; SPI, soybean protein isolate; R, stability coefficient.

droplets and the aggregation of SPI at elevated temperatures (Xu et al., 2018). Moreover, there was no significant difference in the Z-average diameter between NEs at the same temperature (Fig. 3F). According to Fig. 3**G**, no significant change in the zeta-potential was found during thermal treatment, indicating that heating did not strongly affect the structure of NEs. The R values decreased from 92.38 % to 76.64 % as the temperature rose from 24 °C to 100 °C, which was attributed to the droplet flocculation (Fig. 3**H**). Therefore, the DIO-SPI NEs remained stable at low temperatures. Falleh et al., (2021b) reported that the average droplet size of peppermint and myrtle NEs increased as temperatures ranged from 4 °C to 100 °C. Falleh et al., (2021a) demonstrated that cinnamon and clove NEs were stable at 4, 25, 60, or 105 °C, with the average droplet size ranging from 146.2 nm to 165.7 nm.

3.4.5. Storage stability

As shown in Fig. 4**A**, the Z-average diameter of the DIO-SPI NEs increased with the prolongation of storage days. At 4 °C, there was no significant difference in the Z-average diameter of the DIO-SPI NEs from the 1st day to the 10th day. After 30 days, the Z-average diameter increased to 500 nm, showing remarkable storage stability. This can be attributed to the droplet's solid and cohesive interfacial film, as well as

the droplet collision rate and frequency being relatively low at 4 °C, which could delay droplet size growth (Fernández-Ávila, Escriu, & Trujillo, 2015). After 30 days of storage at 25 °C and 37 °C, the Z-average diameter of the NEs increased significantly, reaching about 3047 nm and 4042 nm at the 30th day, and the DIO-SPI NEs were stratified with white flocs. On the same day of storage during 15 ~ 30 days, the Z-average diameter of the NEs at 37 °C changed significantly compared to that at 25 °C or 4 °C (p < 0.05). This phenomenon can be attributed to protein denaturation and thermal aggregation, Brownian motion, gravitational forces, and the Ostwald ripening phenomenon (Falleh et al., 2021b; Tian et al., 2021; Yan Zhou et al., 2020). Our results were consistent with the conclusions reported by Fernández-Ávila et al. (2015), Zhou et al. (2020), and Bi et al. (2023), but inconsistent with Cortés-Muñoz et al. (2009). Fernández-Ávila et al. (2015) and Zhou et al. (2020) both found that SPI NEs were stable at 4 °C. Bi et al. (2023) observed that curcumin NEs became turbid when stored at 55 °C for 7 days, with particle sizes exceeding 200.00 nm. Cortés-Muñoz et al. (2009) reported an increase in particle size of whey NEs when stored at 4 °C for 15 days.

Fig. 4**C** showed that the PDI of DIO-SPI NEs was relatively uniform after 30 days of storage at 4 °C, remaining below 0.4. However, at 25
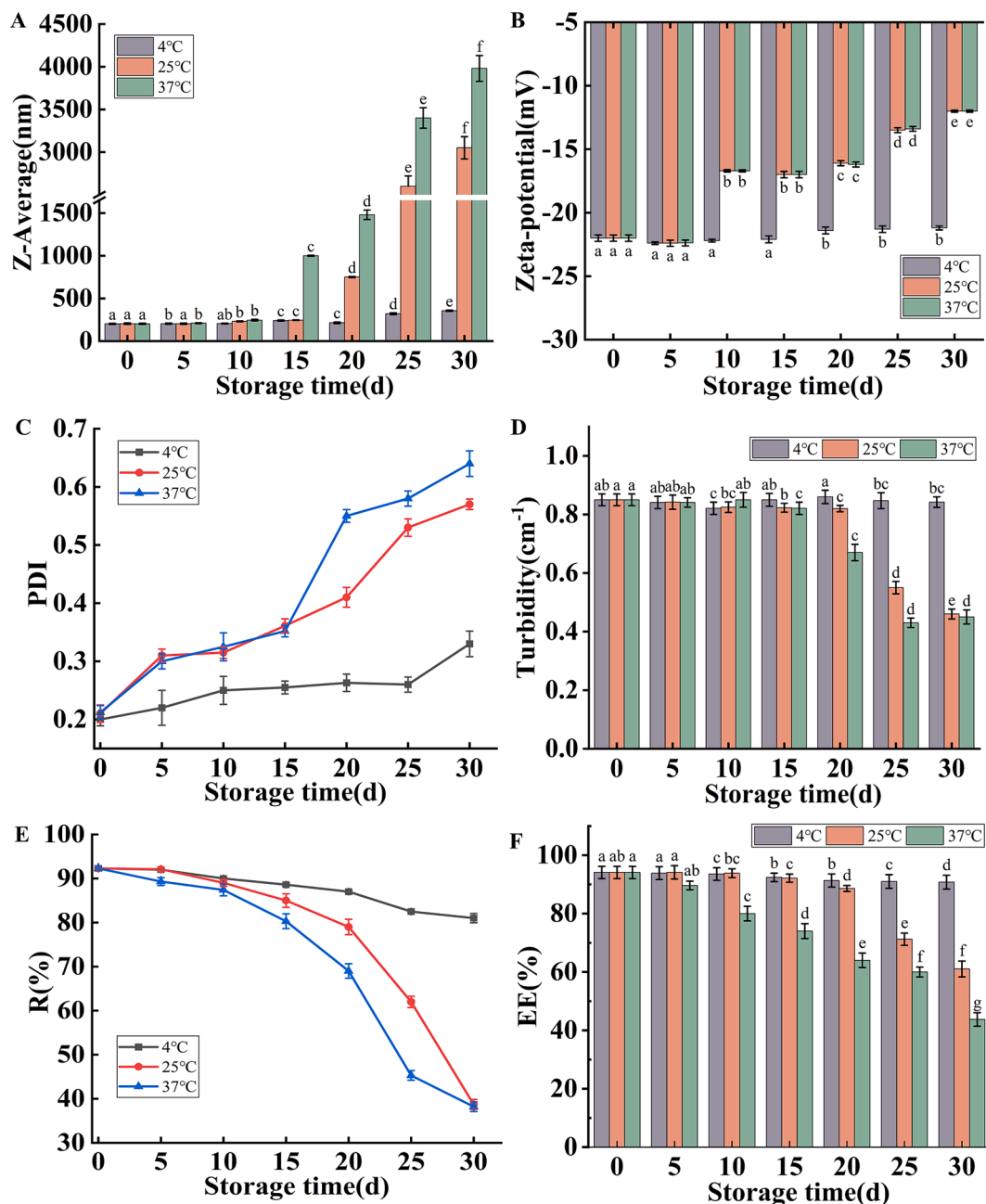
Fig. 4. Storage stability of DIO-SPI NEs. Z-Average(A), zeta-potential (B), PDI (C), turbidity(D), R (E), and EE (F). Bars (mean ± std dev, n = 3) with different letters have mean values that are significantly different (p < 0.05). DIO, diosgenin; NEs, nanoemulsions; SPI, soybean protein isolate; PDI, polydispersity index; R, stability coefficient; EE, encapsulation efficiency.

and 37 °C, the PDI increased significantly with the prolongation of storage time, reaching 0.57 and 0.64, respectively. Higher storage temperatures accelerated the diffusion of surfactant from the oil–water interfacial layer to the aqueous phase, forming larger oil droplets. The absolute Zeta-potential of NEs gradually decreased from 22 mV to 21.2, 12.0, and 12.0 mV after being stored at 4, 25, and 37 °C for 30 days, respectively (**Fig. 4B**).

The turbidity and R of the DIO-SPI NEs during 30 days of storage are shown in **Fig. 4D and E**. The turbidity ranged from 0.85 to 0.43 cm^{-1} during the 30 days. There was no significant difference in the turbidity of the NEs from the 1st day to the 15th day. The DIO-SPI NEs at 4 °C for 30 days remained emulsion, with minor change in turbidity. However, after 20 days, the NEs stored at 25 °C and 37 °C were stratified, resulting in a significant decrease in turbidity (0.42 and 0.38 cm^{-1} at the 30th day). The R decreased as the storage time extended. After 30 days, the R decreased by 11.3 % (4 °C), 53.6 % (25 °C), and 54.1 % (37 °C), respectively. These results indicated that the Ostwald maturation occurred when the NEs were stored at a high temperature for a long time, decreasing in shelf life.

The EE of the DIO-SPI NEs decreased during storage (Fig. 5F). The initial EE of the DIO-SPI NEs was 94.09 %. After storage for 30 days, the EE decreased to 90.77 % (4 °C), 61.03 % (25 °C), and 43.76 % (37 °C), respectively. There was a significant difference in EE between the 0 days and the 30th day at all three temperatures (4 °C, 25 °C or 37 °C). On the 30th day, the EE of the DIO-SPI NEs at 4 °C significantly differed from that at both 25 °C and 37 °C. These results can be explained by the fact that the emulsification of the SPI decreased with increasing storage time, resulting in no more SPI covering the oil–water interface. Moreover,
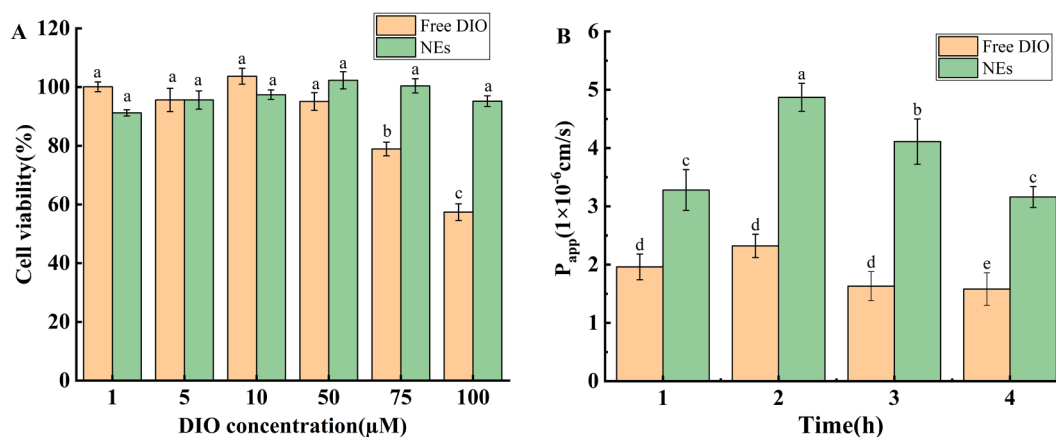
Fig. 5. (A) Cytotoxicity effect of DIO-SPI NEs and free DIO using MTT assay; (B) apparent cell permeability coefficient of DIO-SPI NEs and free DIO. Bars (mean ± std dev, n = 3) with different letters have mean values that are significantly different (p < 0.05). DIO, diosgenin; NEs, nanoemulsions.

higher temperatures accelerated coagulation and precipitation, leading to a decrease in EE. Our findings agreed with Liu et al. (2021), who showed that the retention rate of cinnamon essential oil NEs was above 80 % after storage at 4 °C for 20 days.

3.5. Cytotoxicity

The cytotoxicity of the DIO-SPI NEs was determined using MTT assay, and the results are shown in Fig. 5A. With the concentration of free DIO increasing from 1 to 100 μM, cell viability (%) decreased from 95.00 % to 57.00 %. However, the cell viability of the DIO-SPI NEs was above 90 %. At the same concentration, Caco-2 cells treated with the DIO-SPI NEs exhibited significantly higher survival rate than those treated with free DIO. This may be due to NEs encapsulating the DIO, thereby reducing cell injury caused by the free DIO. In addition, the protective effect of NEs on DIO might delay its release in cells (W. Wang et al., 2017). This result was similar to the study, which found lower cytotoxicity of quercetin-rice bran protein NEs compared to free quercetin after 24 h of treatment (Chen et al., 2020). When the DIO-SPI NEs or DIO concentration was 1 ~ 10 μM, the cell survival rate was above 90 %, indicating no adverse side effects on the cells. Therefore, 10 μM was selected for the cell transport experiments.

3.6. Apparent permeability coefficient

As shown in Fig. 5B, the apparent permeability coefficient of the DIO-SPI NEs ranged from 3.16×10^{-6} to 4.87×10^{-6}, while it ranged from 2.32×10^{-6} to 1.58×10^{-6} for the free DIO. Moreover, the apparent permeability coefficient of the DIO-SPI NEs was significantly higher than that of free DIO (p < 0.05). Especially at 2 h, the apparent permeability coefficient of the DIO-SPI NEs was 2.4 times higher than that of free DIO (p < 0.05). This could be attributed to the small size of NEs, which provided a large surface area for interaction with Caco-2 cells, thereby enhancing transport efficiency (Zhang, Field, Vine, & Chen, 2015). These results indicated that DIO-SPI NEs reduced DIO's cytotoxicity and improved its apparent cell permeability coefficient. The results were in agreement with Chen et al. (2020) and Walia *et al.* (2020). Chen et al. (2020) reported that encapsulation of quercetin in rice bran protein-based NEs reduced its toxicity to cells and enhanced its penetration into cells, reaching a rate of 4.93×10^{-6} cm/s. Walia *et al.* (2020) showed that the vitamin D transport efficiency for pea protein-based NEs (233 nm) was 5.3 times greater than that of free vitamin D.

4. Conclusions

DIO-loaded O/W NEs stabilized by SPI were prepared. The results

showed that the concentrations of DIO (0.8 ~ 1.2 mg/mL) significantly affected the physiochemical properties of NEs. The SPI NEs loaded with 1 mg/mL of DIO showed a lower Z-average diameter (209 nm) and higher encapsulation efficiency (94.9 %). Moreover, DIO-SPI NEs exhibited better stability at pH (<4 or > 5), NaCl concentrations (≤0.3 M), temperature treatment (≤60℃), and freeze–thaw cycles (≤2), and as well as storage at 4 °C for 30 days. In addition, NEs showed 1.63 ~ 2.4 times greater transport efficiency of DIO across Caco-2 cells than free DIO suspension. Further research would be taken to explore the biological activity of DIO-SPI NEs in vivo.

CRediT authorship contribution statement

Li Guanghui: Methodology, Writing – original draft. **Liu Qi:** Investigation, Methodology. **Gao Anning:** Validation. **Ren Luting:** Investigation. **Zhang Yinghan:** Investigation, Validation. **Guo Weiyun:** Conceptualization, Writing – review & editing. **He Shenghua:** Validation, Formal analysis. **Gao Fengyi:** Writing – review & editing, Project administration. **Peng Xiaoli:** Conceptualization, Supervision, Funding acquisition.

Declaration of Competing Interest

The authors declare that they have no known competing financial interests or personal relationships that could have appeared to influence the work reported in this paper.

Data availability

No data was used for the research described in the article.

References

Artiga-Artigas, M., Acevedo-Fani, A., & Martín-Belloso, O. (2017). Effect of sodium alginate incorporation procedure on the physicochemical properties of nanoemulsions. *Food Hydrocolloids, 70*, 191–200.

Bi, D., Li, M., Yao, L., Zhu, N., Fang, W., Guo, W., … Xu, X. (2023). Enhancement of the chemical stability of nanoemulsions loaded with curcumin by unsaturated mannuronate oligosaccharide. *Food Chemistry, 414*, Article 135670.

Bu, G., Zhao, C., Wang, M., Yu, Z., Yang, H., & Zhu, T. (2023). The development and properties of nanoemulsions stabilized with glycated soybean protein for carrying β-carotene. *Journal of Food Engineering, 111411*.

Chen, W., Ju, X., Aluko, R. E., Zou, Y., Wang, Z., Liu, M., & He, R. (2020). Rice bran protein-based nanoemulsion carrier for improving stability and bioavailability of quercetin. *Food Hydrocolloids, 108*, Article 106042.

Cortés-Muñoz, M., Chevalier-Lucia, D., & Dumay, E. (2009). Characteristics of submicron emulsions prepared by ultra-high pressure homogenisation: Effect of chilled or frozen storage. *Food Hydrocolloids, 23*(3), 640–654.

El Fagui, A., & Amiel, C. (2012). PLA nanoparticles coated with a β-cyclodextrin polymer shell: Preparation, characterization and release kinetics of a hydrophobic compound. *International journal of pharmaceutics, 436*(1–2), 644–651.

Falleh, H., Jemaa, M. B., Neves, M. A., Isoda, H., Nakajima, M., & Ksouri, R. (2021a). Formulation, physicochemical characterization, and anti-E. coli activity of food-grade nanoemulsions incorporating clove, cinnamon, and lavender essential oils. *Food Chemistry, 359*, Article 129963.

Falleh, H., Jemaa, M. B., Neves, M. A., Isoda, H., Nakajima, M., & Ksouri, R. (2021b). Peppermint and Myrtle nanoemulsions: Formulation, stability, and antimicrobial activity. *Lwt, 152*, Article 112377.

Fernández-Ávila, C., Escriu, R., & Trujillo, A. (2015). Ultra-high pressure homogenization enhances physicochemical properties of soy protein isolate-stabilized emulsions. *Food Research International, 75*, 357–366.

Geng, M., Feng, X., Wu, X., Tan, X., Shang, B., Huang, Y., … Li, Y. (2023). Characterization and utilization of soy protein isolate–(−)-epigallocatechin gallate–maltose ternary conjugate as an emulsifier for nanoemulsions: Enhanced physicochemical stability of the β-carotene nanoemulsion. *Food Chemistry, 417*, Article 135842.

Gonçalves, R. F., Vicente, A. A., & Pinheiro, A. C. (2023). Incorporation of curcumin-loaded lipid-based nano delivery systems into food: Release behavior in food simulants and a case study of application in a beverage. *Food Chemistry, 405*, Article 134740.

Heydari Gharehcheshmeh, M., Arianfar, A., Mahdian, E., & Naji-Tabasi, S. (2021). Production and evaluation of sweet almond and sesame oil nanoemulsion and their effects on physico-chemical, rheological and microbial characteristics of enriched yogurt. *Journal of Food Measurement and Characterization, 15*, 1270–1280.

Hu, M., Xie, F., Zhang, S., Li, Y., & Qi, B. (2020). Homogenization pressure and soybean protein concentration impact the stability of perilla oil nanoemulsions. *Food Hydrocolloids, 101*, Article 105575.

Jin, Y., Li, F., Lou, X., Xiao, Y., Wang, X., Liu, F., … Xu, H. (2021). Evaluation of the encapsulation capacity of nervous acid in nanoemulsions obtained with natural and ethoxylated surfactants. *Journal of Molecular Liquids, 343*, Article 117632.

Karami-Mohajeri, S., Hashemi, N., Ranjbar, M., Mohajeri, M., & Sharififar, F. (2023). One-Step Preparation of Luteolin Nanoemulsion and Evaluation of its Anti-inflammatory Effect in Animal Models. *Current drug discovery technologies, 20*(3), 45–51.

Li, C., Dai, L., Liu, K., Deng, L., Pei, T., & Lei, J. (2015). A self-assembled nanoparticle platform based on poly (ethylene glycol)–diosgenin conjugates for co-delivery of anticancer drugs. *RSC advances, 5*(91), 74828–74834.

Li, C., Wang, Z., Lei, H., & Zhang, D. (2023). Recent progress in nanotechnology-based drug carriers for resveratrol delivery. *Drug Delivery, 30*(1). https://doi.org/10.1080/10717544.2023.2174206

Liao, W., Gharsallaoui, A., Dumas, E., Ghnimi, S., & Elaissari, A. (2021). Effect of carrier oil on the properties of sodium caseinate stabilized O/W nanoemulsions containing Trans-cinnamaldehyde. *Lwt, 146*, Article 111655.

Liu, C., Chang, J., Zhang, L., Xue, H., Liu, X., Liu, P., & Fu, Q. (2017). Preparation and evaluation of diosgenin nanocrystals to improve oral bioavailability. *AAPS PharmSciTech, 18*, 2067–2076.

Liu, X., Chen, L., Kang, Y., He, D., Yang, B., & Wu, K. (2021). Cinnamon essential oil nanoemulsions by high-pressure homogenization: Formulation, stability, and antimicrobial activity. *Lwt, 147*, Article 111660.

López-Monterrubio, D., Lobato-Calleros, C., Vernon-Carter, E., & Alvarez-Ramirez, J. (2021). Influence of β-carotene concentration on the physicochemical properties, degradation and antioxidant activity of nanoemulsions stabilized by whey protein hydrolyzate-pectin soluble complexes. *Lwt, 143*, Article 111148.

Marhamati, M., Ranjbar, G., & Rezaie, M. (2021). Effects of emulsifiers on the physicochemical stability of Oil-in-water Nanoemulsions: A critical review. *Journal of Molecular Liquids, 340*, Article 117218.

Okawara, M., Hashimoto, F., Todo, H., Sugibayashi, K., & Tokudome, Y. (2014). Effect of liquid crystals with cyclodextrin on the bioavailability of a poorly water-soluble compound, diosgenin, after its oral administration to rats. *International journal of pharmaceutics, 472*(1–2), 257–261.

Pandey, S. K., Patel, D. K., Thakur, R., Mishra, D. P., Maiti, P., & Haldar, C. (2015). Anti-cancer evaluation of quercetin embedded PLA nanoparticles synthesized by emulsified nanoprecipitation. *International journal of biological macromolecules, 75*, 521–529.

Sari, T., Mann, B., Kumar, R., Singh, R., Sharma, R., Bhardwaj, M., & Athira, S. (2015). Preparation and characterization of nanoemulsion encapsulating curcumin. *Food Hydrocolloids, 43*, 540–546.

Semwal, P., Painuli, S., Abu-Izneid, T., Rauf, A., Sharma, A., Daştan, S. D., . . . Das, R. (2022). Diosgenin: an updated pharmacological review and therapeutic perspectives. *Oxidative Medicine and Cellular Longevity, 2022*.

Shahbazizadeh, S., Naji-Tabasi, S., & Shahidi-Noghabi, M. (2022). Development of soy protein/sodium alginate nanogel-based cress seed gum hydrogel for oral delivery of curcumin. *Chemical and Biological Technologies in Agriculture, 9*(1), 41.

Shehzad, Q., Rehman, A., Jafari, S. M., Zuo, M., Khan, M. A., Ali, A., … Hussain, A. (2021). Improving the oxidative stability of fish oil nanoemulsions by co-encapsulation with curcumin and resveratrol. *Colloids and Surfaces B: Biointerfaces, 199*, Article 111481.

Tian, T., Tong, X., Yuan, Y., Lyu, B., Jiang, D., Cui, W., … Jiang, L. (2021). Preparation of benzyl isothiocyanate nanoemulsions by different emulsifiers: Stability and bioavailability. *Process Biochemistry, 111*, 128–138.

Walia, N., & Chen, L. (2020). Pea protein based vitamin D nanoemulsions: Fabrication, stability and in vitro study using Caco-2 cells. *Food Chemistry, 305*, Article 125475.

Wang, W., Wang, B., Liu, S., Shang, X., Yan, X., Liu, Z., … Yu, X. (2017). Bioreducible polymer nanocarrier based on multivalent choline phosphate for enhanced cellular uptake and intracellular delivery of doxorubicin. *ACS applied materials & interfaces, 9*(19), 15986–15994.

Wang, X., Wang, M., Zhao, H., Liu, J., Xing, M., Huang, H., … Wang, J. (2022). Flash nanoprecipitation enables regulated formulation of soybean protein isolate nanoparticles. *Food Hydrocolloids, 131*, Article 107798.

Wu, F.-C., & Jiang, J.-G. (2019). Effects of diosgenin and its derivatives on atherosclerosis. *Food & function, 10*(11), 7022–7036.

Xu, J., Mukherjee, D., & Chang, S. K. (2018). Physicochemical properties and storage stability of soybean protein nanoemulsions prepared by ultra-high pressure homogenization. *Food Chemistry, 240*, 1005–1013.

Yang, Y., Wang, B., & Li, B. (2019). Structural requirement of casein peptides for transcytosis through the caco-2 cell monolayer: Hydrophobicity and charge property affect the transport pathway and efficiency. *Journal of agricultural and food chemistry, 67*(42), 11778–11787.

Zhang, J., Field, C. J., Vine, D., & Chen, L. (2015). Intestinal uptake and transport of vitamin B 12-loaded soy protein nanoparticles. *Pharmaceutical Research, 32*, 1288–1303.

Zhou, Y., Teng, F., Tian, T., Sami, R., Wu, C., Zhu, Y., … Li, Y. (2020). The impact of soy protein isolate-dextran conjugation on capsicum oleoresin (Capsicum annuum L.) nanoemulsions. *Food Hydrocolloids, 108*, Article 105818.

Zhou, Y., Yue, W., Luo, Y., Luo, Q., Liu, S., Chen, H., … Zhang, Q. (2022). Preparation and stability characterization of soybean protein isolate/sodium alginate complexes-based nanoemulsions using high-pressure homogenization. *Lwt, 154*, Article 112607.

Zhu, P., He, J., Huang, S., Han, L., Chang, C., & Zhang, W. (2021). Encapsulation of resveratrol in zein-polyglycerol conjugate stabilized O/W nanoemulsions: Chemical stability, in vitro gastrointestinal digestion, and antioxidant activity. *Lwt, 149*, Article 112049.